

The low temperature elastic anomalies in solid helium

Eric Varoquaux*

CNRS and CEA-IRAMIS-DRECAM, Service de Physique de l'État Condensé,
Centre d'Études de Saclay, 91191 Gif-sur-Yvette Cedex (France)

(Dated: March 2010)

The elastic properties of hcp ^4He samples have been shown to display various anomalies. The elastic shear modulus stiffens and the moment of rotational inertia drops when the temperature is lowered below ~ 0.2 K. The relation between these two quantities is studied within the framework of classical deformable-body mechanics. A model based on the formation by plastic flow of extremely soft two-dimensional layers of dislocations is studied analytically and numerically. This model accounts quantitatively for a number of experiments. Other situations, in which it may seem less relevant, are discussed.

I. INTRODUCTION

Helium makes an intriguing solid. Both isotopes ^4He and ^3He crystallise from the liquid at very low temperature under a pressure of 24.5 and 34.5 bar for each isotope respectively.¹ They form at low temperature very soft, highly deformable hexagonal close-packed (hcp) crystals with similar elastic properties. For instance, the transverse sound velocity close to the melting curve extrapolates at absolute zero to ~ 250 m/s: shear waves in the solid propagate hardly any faster than longitudinal sound in the liquid phase. Particles exchange at a high rate in the very soft helium crystal, in both the bosonic and the fermionic solid, owing to the lightness of the helium isotopes. This softness of the helium crystal makes it very prone to plastic deformation and the formation of dislocation lines.

Because of the fast boson exchange in solid ^4He and the presence of defects, the possibility that a Bose-Einstein condensate would form within the crystalline lattice below a certain temperature was raised by a number of authors, starting with Penrose and Onsager in the late fifties.² These authors argued that superfluid coherence, or off-diagonal long-range order (ODLRO), would not occur in an ideally perfect crystal but possibly could in a distorted lattice. Although the proof they gave of that statement was criticised by other authors,^{3–5} it marked the beginning of a long-lasting search, both theoretical and experimental, for features that could reveal the existence of such a “supersolid” state. A specific model for supersolidity based on the Bose-Einstein condensation of vacancies was proposed by Andreev and Lifshits³. This search received a strong impetus after the observation by Kim and Chan (see the reviews⁶) of an anomaly in the rotational inertia of ^4He solid samples as seen as a period shift in torsional oscillators (TO). The increase in the period of the oscillator resonance, now observed by many groups below a temperature of ~ 0.2 K is taken to signal the decoupling of part of the helium mass from the motion of the oscillator bob. This effect, first discussed

by Leggett⁵ and called non-classical rotational inertia (NCRI), occurs in a number of experimental cells with widely different sizes and geometries, including very confined geometries such as those of Vycor, sintered gold In the time-honoured two-fluid model for superfluidity⁷, it would correspond to the appearance of a superfluid fraction in the solid, which would settle to rest and decouple from the oscillator walls as the temperature is reduced. This interpretation is born out by the fact that, if the oscillator geometry is modified by a partition blocking the closed loop along which the superflow is supposed to take place^{8,9}, the effect disappears. Also, it is not observed when the oscillator is filled with ^3He instead of ^4He ,^{8,10} which constitutes a strong hint that quantum statistics plays a fundamental role.

The TO measurements do suggest that some form of superfluid behaviour takes place solid ^4He below $0.1\sim 0.2$ K but other unambiguous manifestations of the existence of a true superfluid component, such as a non-dissipative DC-flow^{11–14} or a persistent current, a second sound mode,¹⁵ the fountain effect, etc ... are still lacking in spite of the efforts and ingenuity of many research groups.

Shear modulus measurements in solid helium at low temperature provide another class of anomalous elastic properties. These measurements span many years, starting with the early work of Wanner *et al.*¹⁶ soon followed by others.^{17–21} They have recently been extended to the same range of temperatures and impurity concentrations as those with torsional oscillators^{22–25}. A marked decrease in the shear modulus G takes place in most samples of solid ^4He upon warming from $T \sim 0$. The magnitude of the softening varies from sample to sample, depending in particular on the ^3He impurity content x_3 and the cooling history. The drop in G can be anomalously large, up to 60^{17,24} to 80 %²⁵ from the low temperature value of G . Day and Beamish²² have argued that these T and x_3 dependence were mimicking closely those of the period shifts in TO experiments. In fact, the striking similarities between the shear modulus and the NCRI fraction drops make it hard not to believe that the two phenomena are somehow related.

This article outlines one possible such connection between those two different mechanical properties of

* eric.varoquaux@cea.fr

solid helium. It differs from similar attempts by other workers²⁶ with diverging conclusions²⁷ because it recognises from the start that the large drop in G requires the bunching of dislocation lines into extended quasi-planar highly deformable sheets, as described in Sec.(II). The consequences of these assumed planar defects are derived analytically for the shear modulus drop and for the apparent change of inertia in Sec.(III). Those two quantities are thus directly linked to one another. Numerical values are derived in Sec.(IV), where it is shown that this simple model can account quantitatively for most experimental observations. The model does not explain readily certain classes of experiments, notably those in confined geometries, and also the absence of inertia anomaly in solid ^3He . Some speculations on these problems are offered in the last Section.

II. THE SOFT LAYER MODEL

II.1. Planar layers of dislocations

Early sound propagation studies in hcp ^4He in the 5-50 MHz frequency range^{16,19,28,29} have revealed a large temperature dependence of the transverse sound velocity c_T that has been interpreted as arising from the motion of dislocation lines. Analysing the results in the framework of the Granato-Lücke theory,³⁰ as is done with the help of the following relation

$$G/G_{\text{eff}} = 1 + 24(1 - \nu)\Omega\Lambda L^2/\pi^3, \quad (1)$$

together with an expression for the dissipation due to dislocation motion, yields the density of dislocation lines Λ and the average distance between the nodes of the dislocation network L , assuming a value of 0.3 for the Poisson ratio ν and taking the highest value for the orientation parameter $\Omega \leq 1/2$. The values of these parameters derived from sound propagation measurements in the megahertz range typically lie in the range $10^4 \sim 10^6 \text{ cm}^{-2}$ for Λ and $5 \cdot 10^{-4} - 10^{-3} \text{ cm}$ for L .

Lower frequency measurements^{17,21}, interpreted in the same manner give substantially higher values of the quantity $\Omega\Lambda L^2$ 1.4 - 2.3^{17,18} at 15 and 78 kHz, and therefore of ΛL^2 , of the order of 3 or more. The shear modulus measurements by Paalanen *et al.*²¹ were carried out at a low frequency of 331 Hz and lead to a value of ΛL^2 , $\gtrsim 1.0$ to 2.5 depending on samples. These values are much larger than those obtained from high frequency sound propagation measurements, carried out above the mean resonance frequency of individual dislocation lines, estimated to be around 100 kHz²¹. More recent measurements^{22,24,31,32} have confirmed these results. A softening of 86 % has been observed in a high quality, ultra-pure ^4He sample by Rojas *et al.*²⁵ at frequencies in the 10-20 kHz range. In this extreme situation, the quantity ΛL^2 would exceed 20 with the same values as above for the Poisson ratio ν and the orientation parameter Ω .

Such high values of ΛL^2 , and the discrepancy between high and low frequency values, point towards the formation of inhomogeneous dislocation structures, such as the mosaic in which the dislocation lines crop along the boundaries between grain with slightly misaligned lattice vectors³³, or more extended planar structures, as discussed below. This remark provides the basis for what follows : the observed extreme softening in solid ^4He will be taken to be due to the formation of planar layers of parallel dislocation lines, which become extremely compliant under shear stress.

These planar defects have been observed in a number of metallurgical samples³³ as well as in hcp ^4He by X-ray topography by Iwasa *et al.*^{34,35}. Their formation and detailed morphology have been studied by numerical simulations of how the dislocations organise themselves dynamically into various spatially heterogeneous structures under various applied stress or strain rate conditions^{36,37}. Depending on the sample history and geometry, dislocations collect into slip bands, planar arrays and dislocation cells. This phenomenon is assumed here to take place during the formation of the hcp ^4He samples.

II.2. Thermally activated dislocation unpinning

The variation of the shear modulus with temperature, a softening of solid ^4He upon warming, is attributed to the unpinning of the dislocation lines as the trapped ^3He impurities escape from the dislocation cores by thermal activation. This picture is well documented through the work of many authors^{18,20,21} and, more recently, by Syshchenko *et al.*³⁸. These last authors produced from their measurements of the shear elastic modulus in terms of temperature and frequency a particularly interesting graph that shows that the dynamical process behind the softening is thermally activated over an energy barrier of $\sim 0.7 \text{ K}$, which is the binding energy of ^3He impurities to dislocation cores. The data of Syshchenko *et al.*³⁸, together with data from other groups higher temperatures and frequencies, are reproduced Fig.1, which brings further convincing evidence that the shear modulus anomaly is due to the gradual freeing of dislocation lines as ^3He impurities evaporate from their cores.

The simple mechanical system to be discussed below is based on the following scenario. During the cool-down, plastic flow takes place, which produces dislocation lines. These lines bunch together in quasi-planar structures along the plastic flow streamlines. These arrays are densely packed. Dislocations interact strongly and become extremely mobile when they are rid of the ^3He impurities that hamper their motion.

As depicted in Fig.2, the helium sample is supposed to be confined between two parallel plane walls located at $z = 0$ and $z = R$ and extending to infinity along the x and y axes. Shear stresses and strains are produced in the sample either by moving one plane, *e.g.*, that at $z = 0$, which would be the transmitter in the shear mod-

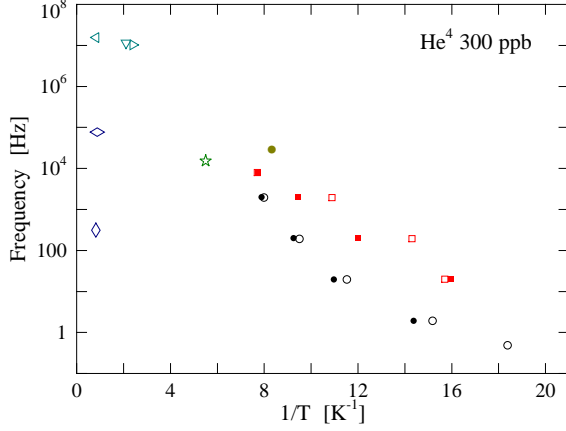


FIG. 1. Frequency in Hz, on a logarithmic scale, *vs* the inverse temperature in K^{-1} at which 50 % of the modulus change has occurred (open symbols); closed symbols are for the dissipation peaks; \triangle pointing right darkcyan Tsuruoka and Hiki²⁹; \triangle downward darkcyan Iwasa *et al.*¹⁹; \triangle left darkcyan Wanner *et al.*¹⁶; tall \diamond darkblue M.A. Paalanen, D.J. Bishop, and H.W. Dail²¹; broad \diamond darkblue Tsymbalenko¹⁷; \star darkgreen Mukharsky *et al.*²⁴; \bullet darkyellow Rojas *et al.*²⁵; Other data points Syshchenko *et al.*³⁸. The general trend of the data corresponds to an activated process over an energy barrier of ~ 0.75 K. The samples are nominal purity ^4He except for the experiments of Rojas *et al.*²⁵.

ulus experiment, with respect to the $z = R$ plane, held steady, and which would then be the receiver. The deformation u induced in the sample depends on z and t only : the problem is one-dimensional and easily solvable. Torsional oscillator experiments are mimicked by moving both bounding walls in unison, letting the sample inertia develop internal stresses.

II.3. Homogeneous solid sample

If the helium sample is homogeneous with a density ρ and a shear modulus G independent of position and time (no visco-elastic effect), the deformation $u(z, t)$ obeys the following partial differential equation ;

$$\rho \frac{\partial^2 u}{\partial t^2} = G \frac{\partial^2 u}{\partial z^2}. \quad (2)$$

This equation describes the propagation of transverse plane waves with dispersion relation $\omega^2 = c_T^2 k^2$, with $c_T^2 = G/\rho$. The harmonic solution of Eq.(2) at ω is the sum of two counter-propagating waves and reads:

$$u(z, t) = (u_{0+} e^{-ikz} + u_{0-} e^{ikz}) e^{i\omega t} = u(z) e^{i\omega t}. \quad (3)$$

The time dependence separates from the spatial dependence and, unless specifically required, will be left out in the following.

The boundary conditions at $z = 0$ and $z = R$ depend on the experiment. For the shear modulus measurements,

the transmitter wall moves harmonically with amplitude u_0 and the receiver wall remains practically still:

$$\begin{aligned} u(z)|_{z=0} &= u_0 = u_{0+}^s + u_{0-}^s, \\ u(z)|_{z=R} &= 0 = u_{0+}^s e^{-ikR} + u_{0-}^s e^{ikR}. \end{aligned} \quad (4)$$

The constants of integration for shear measurements u_{0+}^s and u_{0-}^s are then given by

$$\frac{u_{0+}^s}{e^{ikR}} = \frac{-u_{0-}^s}{e^{-ikR}} = \frac{u_0}{e^{-ikR} - e^{ikR}} = \overline{u_0}, \quad (5)$$

and the solution of Eq.(3) for the deformation as a function of z can then be expressed under the following form:

$$u(z) = \overline{u_0} \left(e^{ik(R-z)} - e^{-ik(R-z)} \right) = u_0 \frac{\sin k(R-z)}{\sin kR}. \quad (6)$$

The stress in the solid is derived from the deformation, still disregarding the time dependence:

$$\begin{aligned} \sigma(z) &= G \frac{du}{dz} = -ik \overline{u_0} G \left(e^{ik(R-z)} + e^{-ik(R-z)} \right) \\ &= -ku_0 G \frac{\cos k(R-z)}{\sin kR}. \end{aligned} \quad (7)$$

The force per unit area acting on the receiver is the opposite of that acting on the body, namely the internal stress:

$$F_R = -\sigma(R) = \frac{ku_0 G}{\sin kR}, \quad (8)$$

so that the effective shear elastic modulus that is measured is such that:

$$\frac{G}{G_{\text{eff}}} = \frac{u_0}{R} \frac{G}{F_R} = \frac{\sin kR}{kR} \simeq 1 - \frac{\rho \omega^2 R^2}{6G} + \dots \quad (9)$$

Equation (9) describes the change of the effective shear modulus at finite frequency due to the elastic response of the body. In the limit $\omega \rightarrow 0$, G_{eff} reduces to G . For $kR = \pi/2$, the body is set into resonance and the effective shear modulus diverges.

This elastic response of the body becomes the dominant effect for inertia measurements, such as those in torsional oscillators, in which the two walls at $z = 0$ and $z = R$ are set into identical motion $u_0 e^{i\omega t}$. The solution to Eq.(2) that satisfies the boundary conditions

$$u(z)|_{z=0} = u(z)|_{z=R} = u_0 \quad (10)$$

can be written with the help of the following relations

$$\frac{u_{0+}^M}{1 - e^{ikR}} = \frac{-u_{0-}^M}{1 - e^{-ikR}} = \frac{u_0}{e^{-ikR} - e^{ikR}} = \overline{u_0}. \quad (11)$$

In particular, the stress $\sigma(z)$ is found to be:

$$\sigma(z) = G \frac{du}{dz} = -kGu_0 \frac{\cos k(R-z) - \cos kR}{\sin kR}. \quad (12)$$

What is measured in the TO type of experiments is the back-action of the sample on the measuring device,

namely the total force $F_X + F_R$ exerted by the solid helium on both the transmitter wall and the receiver wall. This force reads, per unit area,

$$F_X + F_R = \sigma(0) - \sigma(R) = 2kGu_0 \frac{1 - \cos kR}{\sin kR} \quad (13)$$

$$= 2kGu_0 \tan \frac{kR}{2} = \rho\omega^2 Ru_0 \left[1 + \frac{\rho\omega^2 R^2}{12G} + \dots \right].$$

The meaning of Eq.(13) above is made clear by its last member: $\omega^2 u_0$ is the acceleration amplitude, ρR the “bare” inertial mass M_I per unit area and, in the square bracket, the elastic correction at finite frequency. This “effective mass” correction increases with frequency up to the resonance at $kR = \pi$ where it becomes very large.

The shear modulus and effective mass corrections are of the same order of magnitude. Taking, e.g., $R = 1$ cm, a frequency of 1 kHz, $\rho = 0.194$ g/cm³ and $c_T = 267$ m/s, they are not insignificant, being of the order of 1%, but they do not depend on temperature if dislocations are not brought into the picture, which will now be considered.

II.4. Soft layers

As mentioned in the Introduction helium makes crystals that are very soft - the longitudinal and transverse sound velocities are low - and very fragile - the yield strength is small. Dislocations appear readily under very weak mechanical or thermal perturbations. Plastic flow, during which dislocations form, takes place during the formation of the solid helium sample and the subsequent cooling. It has been shown by numerical simulations, notably by Amadeo and Ghoniem³⁶, that these dislocations collect in different planar structures according to different applied perturbations. Planar arrays composed of sets of dislocation dipoles lying in planes containing the direction of the critical resolved shear stress form under monotonic stress conditions. Other types of structures, slip bands or dislocation cells, may also appear. These regions with a high dislocation density are very soft and deform very easily. They separate regions with depleted dislocation densities in which deformation processes occur far less readily.

These structures are thicker than the Franck networks that separate two low-tilt grain boundaries. They are quite different from the random network assumed in the Granato-Lücke model³⁰.

To account for the effect of dislocations, two such highly deformable structures are introduced at z_1 and z_2 parallel to the boundaries as depicted in Fig.2 to account for the shear modulus anomaly discussed above. Strain and stress are continuous functions at the interface between the slab of dislocation-poor crystal and the soft layer. Denoting the shear modulus in the soft layer G_s , shear plane waves propagate with wave vector $k_s = \sqrt{\rho/G_s}$. The transfer matrix describing the propagation of the vector $[u(z), \sigma(z)]$ in the layer of thickness

d reads

$$\mathbf{M}(d) = \begin{bmatrix} \cos k_s d & (1/k_s G_s) \sin k_s d \\ -k_s G_s \sin k_s d & \cos k_s d \end{bmatrix}.$$

Although the problem of finding how plane waves propagate through the stack of slabs depicted in Fig.2 is formally solved by multiplying transfer matrices such as $\mathbf{M}(d)$, it saves a number of algebraic steps to let the thickness d and the modulus G_s go to zero in such a way that d/G_s remains constant and equal to α and to replace the effect of the soft layer to a discontinuous jump in the deformation proportional to the local stress, described, for the layer at z_1 , by

$$\begin{aligned} u(z_1 + d) &= u(z_1) + \alpha_1 \sigma(z_1), \\ \sigma(z_1 + d) &= -k_s^2 d G_s u(z_1) + \sigma(z_1) = \sigma(z_1), \end{aligned} \quad (14)$$

the last equality holding in the limit $d G_s \rightarrow 0$. These boundary conditions, which could have been anticipated, also apply to the soft layer at z_2 with slip parameter α_2 . In the following, the soft layers will be described by their compliances α_i/R , which are such that the $\kappa_i = \alpha_i G/R$ are dimensionless quantities.

III. ANALYTICAL RESULTS

With the boundary conditions, Eqs.(14), describing the soft layers, the propagation of the propagating and counter-propagating waves through the three slabs of homogeneous crystal with shear modulus G , obeying no-slip boundary conditions at the walls similar to Eqs.(4) for shear or Eqs.(10) for the inertial case, can be found by straightforward, if lengthy, algebra.

III.1. Wave propagation through the sample

The amplitudes of the propagating and counter-propagating waves in region II are linearly related to those in region 0:

$$\begin{aligned} u_{2+} &= \delta_{11} u_{0+} + \delta_{12} u_{0-}, \\ u_{2-} &= \delta_{21} u_{0+} + \delta_{22} u_{0-}. \end{aligned} \quad (15)$$

The wave propagation in slab 0, between $z = 0$ and z_1 as shown in Fig.2, is represented by Eq.(3), which involves two integration constants u_{0+} and u_{0-} , the amplitudes of the counter-propagating plane waves with pulsation ω and wave-vector k and $-k$. Similar solutions obtain in slab I, between z_1 and z_2 , and slab II between z_2 and $z = R$, involving constants u_{1+} , u_{1-} , and u_{2+} , u_{2-} respectively.

The deformation discontinuity at the soft layer at z_1

yields the following relations:

$$u_1(z_1) = u_{1+}e^{-ikz_1} + u_{1-}e^{ikz_1} \quad (16)$$

$$= u_{0+}(1 - i\kappa_1 kR)e^{-ikz_1} + u_{0-}(1 + i\kappa_1 kR)e^{ikz_1} ,$$

$$\sigma(z_1) = -ikG(u_{0+}e^{-ikz_1} - u_{0-}e^{ikz_1})$$

$$= -ikG(u_{1+}e^{-ikz_1} - u_{1-}e^{ikz_1}) . \quad (17)$$

Similar relations hold between u_{1+} , u_{1-} , and u_{2+} , u_{2-} . Eliminating u_{1+} and u_{1-} leads the following expressions for the coefficients δ_{ij} of the matrix which describe wave propagation through the stack of slabs 0, I, II:

$$\delta_{11} = \left(1 - i\frac{\kappa_1}{2}kR\right) \left(1 - i\frac{\kappa_2}{2}kR\right) + \frac{\kappa_1\kappa_2}{4}k^2R^2 e^{2ik(z_2 - z_1)} = \delta'_{11} + i\delta''_{11} , \quad (18a)$$

$$\delta_{12} = i\frac{\kappa_1}{2}kR \left(1 - i\frac{\kappa_2}{2}kR\right) e^{2ikz_1} + i\frac{\kappa_2}{2}kR \left(1 + i\frac{\kappa_1}{2}kR\right) e^{2ikz_2} = \delta'_{12} + i\delta''_{12} , \quad (18b)$$

$$\delta_{21} = -i\frac{\kappa_1}{2}kR \left(1 + i\frac{\kappa_2}{2}kR\right) e^{-2ikz_1} - i\frac{\kappa_2}{2}kR \left(1 - i\frac{\kappa_1}{2}kR\right) e^{-2ikz_2} = \delta_{12}^* , \quad (18c)$$

$$\delta_{22} = \left(1 + i\frac{\kappa_1}{2}kR\right) \left(1 + i\frac{\kappa_2}{2}kR\right) + \frac{\kappa_1\kappa_2}{4}k^2R^2 e^{-2ik(z_2 - z_1)} = \delta_{11}^* , \quad (18d)$$

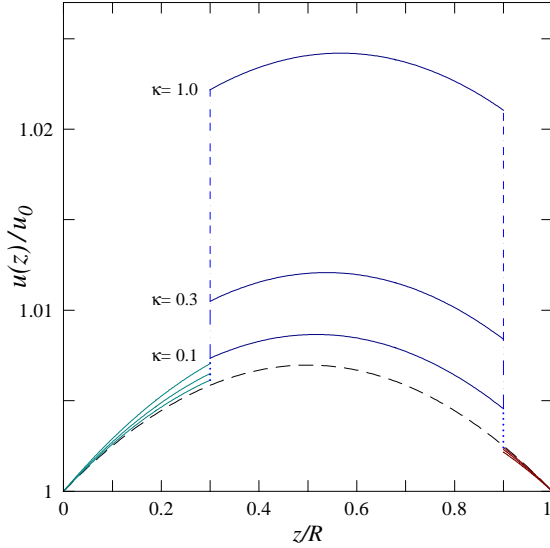


FIG. 2. Forms of the stationary wave pictured as the relative displacement $u(z)/u_0$ for z varying from 0 to R for various dimensionless compliance κ of the soft layers, taken to be equal, for $R = 1$ cm at a frequency of one kHz ($kR = 0.2354$). The soft layers lay at $z_1 = 0.3R$ and $z_2 = 0.9R$, at the interfaces between slab 0, left, slab I, middle, and slab II, right. The dash-dot lines mark the discontinuities of $u(z)$. The dash-dash line represents the elastic behaviour with no soft layers.

The matrix $\Delta = ||\delta_{ij}||$, Eq. (18), describing wave propagation in a conservative time-reversal invariant system, is unitary and has determinant unity:

$$\delta_{11}\delta_{22} - \delta_{12}\delta_{21} = 1 . \quad (19)$$

III.2. The shear modulus

For shear modulus measurements, the no-slip condition at the walls reads:

$$u_{0+} + u_{0-} = u_0 ,$$

$$u_{2+}e^{-ikR} + u_{2-}e^{ikR} = 0$$

$$= (\delta_{11}e^{-ikR} + \delta_{21}e^{ikR})u_{0+} + (\delta_{12}e^{-ikR} + \delta_{22}e^{ikR})u_{0-} ,$$

relations from which the constants u_{0+} and u_{0-} can be derived:

$$\frac{u_{0+}^s}{\delta_{12}e^{-ikR} + \delta_{22}e^{ikR}} = \frac{-u_{0-}^s}{\delta_{11}e^{-ikR} + \delta_{21}e^{ikR}}$$

$$= \frac{u_0}{(\delta_{12} - \delta_{11})e^{-ikR} - (\delta_{21} - \delta_{22})e^{ikR}} = \tilde{u}_0 . \quad (20)$$

The quantities u_{0+}^s and u_{0-}^s expressed by Eqs.(20) now include the effect of the soft layers and should not be confused with those given by Eq.(5), which do not. The shear stress at the receiver $\sigma(R)$ is given by

$$\sigma(R) = G \frac{du}{dz} \Big|_R = -ikG(u_{2+}e^{-ikR} - u_{2-}e^{ikR}) .$$

Expressing u_{2+} and u_{2-} in terms of u_{0+}^s and u_{0-}^s using Eqs.(18) and (19), $\sigma(R)$ takes the following simple form:

$$\sigma(R) = -2ikG\tilde{u}_0 = -kGu_0/\mathcal{D} , \quad (21)$$

with

$$\mathcal{D} = (1/2i) [(\delta_{12} - \delta_{11})e^{-ikR} - (\delta_{21} - \delta_{22})e^{ikR}]$$

$$= \sin kR + \kappa_1 kR \cos k(R - z_1) \cos kz_1$$

$$+ \kappa_2 kR \cos k(R - z_2) \cos kz_2$$

$$- \kappa_1 \kappa_2 k^2 R^2 \sin k(z_2 - z_1) \cos k(R - z_2) \cos kz_1 .$$

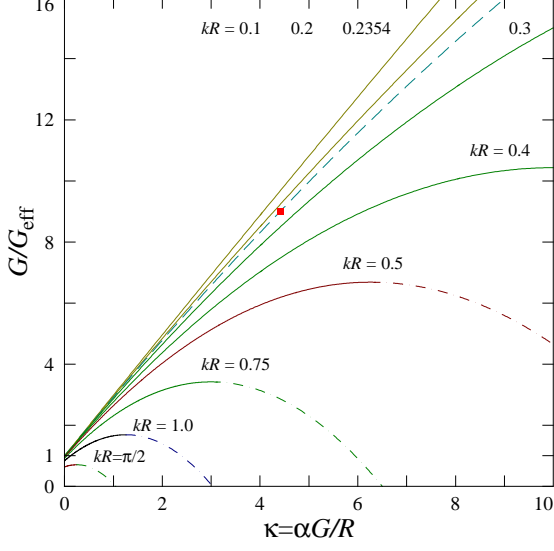


FIG. 3. Inverse effective shear modulus G_{eff} , normalised to the shear modulus with no soft layers G in terms of the dimensionless compliance κ of the soft layers, for the same parameter values as in Fig.2 for various values of kR . The dash-dash curve represents the case with $R = 1$ cm at a frequency of one kHz, $kR = 0.2354$. The symbols mark the cases discussed in the text, (■) for $G/G_{\text{eff}} = 9$, $\kappa = 4.411$, (●) for $G/G_{\text{eff}} = 1.6$, $\kappa = 0.3075$. The dash-dot-dash lines correspond to an unphysical branch of Eq.(22a).

The effective shear modulus $G_{\text{eff}} = -\sigma(R) R/u_0$ follows readily from Eq.(21):

$$\frac{G}{G_{\text{eff}}} = \frac{\mathcal{D}}{kR} \quad (22a)$$

$$\begin{aligned} &\simeq 1 + \kappa_1 + \kappa_2 - \frac{k^2 R^2}{6} - \frac{\kappa_1 + \kappa_2}{2} k^2 R^2 \\ &+ \kappa_1 k^2 z_1 (R - z_1) + \kappa_2 k^2 z_2 (R - z_2) \\ &- \kappa_1 \kappa_2 k^2 R (z_2 - z_1) + \dots \end{aligned} \quad (22b)$$

For typical numerical values, such as those used for the graphs in Fig.2, the first two terms of the expansion of $1/G_{\text{eff}}$ with respect to kR , Eq.(22b), fall within 1% of the exact value given by Eq.(22a). Also, the zeroth order term could have been written from a simple inspection of Fig.2. The correction to the inertial mass turns out to be less transparent.

III.3. Effective mass

The derivation of the effect of the soft layers on the apparent inertia of the sample follows that given in Sec.II.3 for the homogeneous sample, starting from the same boundary conditions, Eqs.(10). Equation (11) for the

integration constants is modified to:

$$\frac{u_{0+}^{\text{M}}}{\delta_{12}e^{-ikR} + \delta_{22}e^{ikR} - 1} = \frac{-u_{0-}^{\text{M}}}{\delta_{11}e^{-ikR} + \delta_{21}e^{ikR} - 1} = \tilde{u}_0, \quad (23)$$

the quantity \tilde{u}_0 being the same as in Eq.(20) for the shear modulus case.

For these integration constants, the stress at each wall reads:

$$\sigma(0) = G \frac{du}{dz} \Big|_{z=0} = -ikG(u_{0+}^{\text{M}} - u_{0-}^{\text{M}}) \quad (24)$$

$$= ikG\tilde{u}_0 \left[2 - (\delta_{12} + \delta_{11})e^{-ikR} - (\delta_{22} + \delta_{21})e^{ikR} \right],$$

$$\begin{aligned} \sigma(R) &= G \frac{du}{dz} \Big|_{z=R} = -ikG(u_{2+}e^{-ikR} - u_{2-}e^{ikR}) \\ &= -ikG\tilde{u}_0 \left[2(\delta_{11}\delta_{22} - \delta_{12}\delta_{21}) \right. \\ &\quad \left. - (\delta_{11} - \delta_{12})e^{-ikR} - (\delta_{22} - \delta_{21})e^{ikR} \right]. \end{aligned} \quad (25)$$

The total force per unit area exerted by the helium sample on both walls is now given, instead of Eq.(13) for the homogeneous case, by

$$F_X + F_R = \sigma(0) - \sigma(R) = 2ikG\tilde{u}_0 \left[2 - \delta_{11}e^{-ikR} - \delta_{22}e^{ikR} \right],$$

using again the property that $||\delta_{ij}||$ has determinant unity. Expliciting the quantities in square brackets with the help of Eqs.(18) and making use of Eq.(22a), the total force on the walls takes the final form

$$F_T = F_X + F_R = kGu_0 \frac{\mathcal{N}}{\mathcal{D}} = \frac{u_0}{R} G_{\text{eff}} \mathcal{N}, \quad (26)$$

with

$$\begin{aligned} \mathcal{N} &= 2 - \delta_{11}e^{-ikR} - \delta_{22}e^{ikR} = 2(1 - \cos kR) \\ &+ (\kappa_1 + \kappa_2)kR \sin kR - \kappa_1 \kappa_2 k^2 R^2 \sin k(z_2 - z_1) \\ &\times \{ \sin k(z_2 - z_1) + \sin k(R - z_2 + z_1) \}. \end{aligned}$$

III.4. Stationary waveforms

The displacement $u(z)$ in the sample can easily be evaluated using, *e.g.* in the inertia measurement case, the solution to the wave equation expressed by Eqs.(23) for u_{0+}^{M} and u_{0-}^{M} , with the following result:

- for slab 0: $u(z)^{(0)} = u_0[\cos kz + (B/A) \sin kz]$,
- for slab I: $u(z)^{(I)} = u_0[\cos kz - \kappa_1 kR/2\{\sin kz + \sin k(2z_1 - z)\} + (B/A)[\sin kz + \kappa_1 kR/2\{\cos kz + \cos k(2z_1 - z)\}]]$,
- for slab II: $u(z)^{(II)} = (u_0/A)[\sin k(R - z) + \sin kR + \kappa_1 kR/2 \cos k(z - z_1) \cos kz_1 + \kappa_2 kR/2 \cos k(z - z_2) \cos kz_2 - \kappa_1 \kappa_2 K^2 G^2 \sin k(z_2 - z_1) \cos k(z - z_2) \cos kz_1]$,

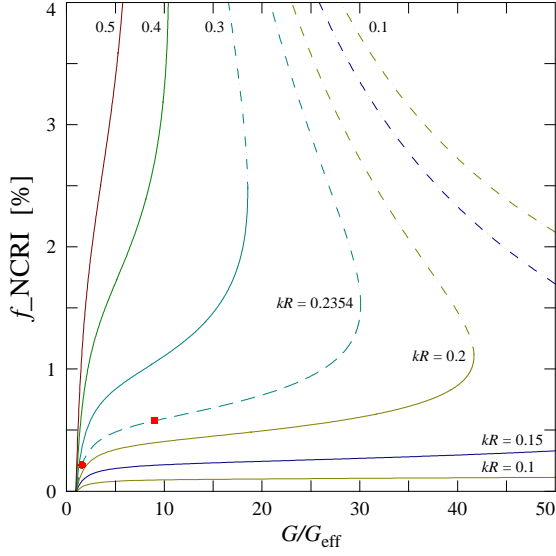


FIG. 4. Relative change in the apparent inertia, f_{NCRI} vs the inverse dimensionless shear modulus G/G_{eff} , for the situation of Fig.(2), for various values of kR as labelled in the figure. The symbols (●) and (■) mark the cases discussed in the text on the dash-dash curve for $kR = 0.2354$. The dash-dot-dash portions of the various curves correspond to the unphysical branch of Eq.(22a)

with

$$A = (\delta'_{11} - \delta'_{12}) \sin kR + (\delta''_{12} - \delta''_{11}) \cos kR = \mathcal{D} ,$$

$$B = 1 - (\delta'_{11} + \delta'_{12}) \cos kR - (\delta''_{12} + \delta''_{11}) \sin kR .$$

These expressions can readily be evaluated numerically. As an example, the relative displacement $u(z)/u_0$ for three values of the dimensionless compliance κ of the soft layers, taken to be equal, is shown in Fig.2 for $kR = 0.2354$, $z_1 = 0.3R$ and $z_2 = 0.9R$. The discontinuities at z_1 and z_2 caused by these soft layers increase in size with the compliance, up to the point where \mathcal{D} becomes zero and the deformation diverges.

The next step, carried out in the following Section, consists in extracting the parameters κ_i of the soft layers from the measured value of G_{eff} and evaluating the corresponding apparent change in inertia.

IV. NUMERICAL RESULTS

If an arrangement of dislocation lines such as depicted in Fig.2 takes place, the change of the effective shear modulus when κ varies entails a correlated change of the internal motion in the system.

The change of G/G_{eff} with temperature, that is, when the softness parameter κ varies from its low temperature value, assumed to be negligibly small because the dislocations are immobilised by the isotopic impurities is relatively straightforward to interpret because its observed

magnitude is large, and because, as seen from Eq.(22b), it is a zeroth order effect in the small parameter kR . That of the effective mass is more difficult to single out because it has a magnitude comparable to that of the plain elastic response, which is not measured and should be subtracted out. This difference reads from Eq.(13) and as Eq.(26) follows:

$$F_T - F_T|_{\kappa_1=\kappa_2=0} = \frac{\rho\omega^2 u_0 R}{kR} \left\{ \frac{\mathcal{N}}{\mathcal{D}} - 2 \frac{1 - \cos kR}{\sin kR} \right\} \quad (27a)$$

$$\simeq \rho\omega^2 u_0 R \frac{k^2 R^2}{1 + \kappa_1 + \kappa_2} \times \left[\frac{\kappa_1 + \kappa_2}{4} - \kappa_1 \frac{z_1(R - z_1)}{R^2} - \kappa_2 \frac{z_2(R - z_2)}{R^2} \right] . \quad (27b)$$

Equations (27a) and (27b) show how what could be called the “superfluid fraction”, $(F_T - F_T|_{\kappa_1=\kappa_2=0})/\rho\omega^2 u_0 R = f_{\text{NCRI}}$, depends on the compliances κ_i , which in turn are related to the effective shear modulus. The quantity $\rho\omega^2 u_0 R$ has already been found in Eq.(13) and stands for the force due to the acceleration of the inertial mass $M_I = \rho R$, being understood that these quantities hold per unit area.

The full development of Eq.(27a) is fairly lengthy and not particularly transparent but evaluates numerically quite readily. The outcome is discussed below. The lowest order correction to this effective mass, Eq.(27b), is second order in kR and linear in the κ_i 's, the term in $\kappa_1 \kappa_2$, of order $(kR)^3$, being discarded. This correction is either positive or equal to zero for the special case $z_1 = z_2 = R/2$, that is, for a vanishing thickness, dangling mass, and, by symmetry, vanishing local stress in slab II.

Equations (27a) and (27b), together with (22a) and (22b), constitute the main result of this work.³⁹

The variation of the shear modulus in terms of the soft layer compliances, taken to be equal, is shown in Fig.3 for various values of kR for the same sample geometry and parameter values as in Fig.2. As the compliance κ increases from zero, assumed to be its $T = 0$ value, the effective shear modulus G_{eff} decreases, the solid becomes softer, up to a point where G/G_{eff} reaches a maximum: the interfaces between slab I and its neighbours becomes so soft that, although the dangling slab swings with increasing amplitude, the stress due to its motion ceases to increase. Beyond this point, a further increase in κ would lower G/G_{eff} because the stress reflected back onto the external boundaries effectively decreases while the displacement of slab I goes on increasing. Upon further increase of κ this situation reaches a breakdown point at which $u(z)^{(I)}$ becomes infinite and G/G_{eff} nil. This branch of $G/G_{\text{eff}}(\kappa)$, shown in Fig.3 cannot be reached by adiabatic turn-on of κ and will be deemed unphysical.

The adiabaticity in the establishment of the steady-state regime has been implicitly assumed above with the total neglect of damping. If, however, damping terms

are introduced in the wave equation, Eq.(2), slab I would be coupled to its neighbours by friction in addition to shear elasticity and the results obtained above would be quantitatively different for very small G_{eff} .

From the measured overall change in G/G_{eff} due to ^3He impurity unpinning, which reaches values of 1.6,^{18,24} up to 9,²⁵ the corresponding values of the compliance of the soft layers can be found from Eq.(22a). From these values, $\kappa = 0.31$ for $G/G_{\text{eff}} = 1.6$, $\kappa = 4.4$ for $G/G_{\text{eff}} = 9$, the NCRI fractions given by Eq.(27a) are 0.22 % and 0.58 % respectively.

The NCRI fraction is plotted directly in terms of the shear modulus in Fig.4. As already discussed, the reentrant branches of the curves $f_{\text{NCRI}}(G/G_{\text{eff}})$ cannot be reached by adiabatic turn-on of κ . For a given kR , it would seem that G_{eff} cannot take arbitrarily low values but the inclusion of damping in the model would probably invalidate this conclusion. It can be expected that, for finite damping, the NCRI fraction would go on increasing with layer softness.

V. DISCUSSION

Because of the very large drop of the shear modulus that is observed in some samples of solid ^4He , it may be surmised that, instead of forming homogeneous networks, dislocations crop into slip bands or quasi-planar arrays of sizable thickness. Meshes of such planar arrays have been observed in the solid sample,³⁴ patterned along the lines of continuous plastic flow that takes place during the solidification of the ^4He sample and its cool-down. They become very soft and even possibly superfluid when the ^3He impurities evaporate from the dislocation cores.

The simple model described above is tractable analytically and provides the link between the shear modulus and the NCRI fraction measurements that leads to values of the NCRI fraction within the range of the observed values, barring the highest ones.⁴⁰ This model explains readily why the NCRI measurements depend so strongly on the sample thermal history:⁴¹ even small changes in the soft layer properties and the interconnection of the channels that they delimit can greatly influence the motion of the dangling masses. From a very different perspective, the mobile features observed in solid ^4He at higher temperatures⁴² can possibly lend support to the model studied here.

A number of experiments would seem to invalidate this model. The TO experiments with a blocked channel show a much reduced NCRI fraction, which is interpreted as a manifestation of some sort of superflow taking place when flow paths are connected in a loop and not when this loop is broken. However, the same considerations apply to the plastic flow lines, which also can form or

not a connected channel through which a dangling mass such as the one modelled by Slab 2 in Fig.2 can move.

TO measurements in confined geometries, Vycor, porous gold, ... would appear to completely invalidate the present approach. If the model is applied to a single pore, for which parameter kR is very small, then indeed, the resulting effect will also be extremely small. However, the plastic flow pattern extends through out the finely divided interconnected channels. It is unclear whether the characteristic dimension of the sample R should be the size of the fine pores, which would miss the correlation between the various channels, or the overall dimension of the sample.

Kim et al⁴³ experimentally address the connexion between shear and NCRI and conclude that the response to an increase in drive amplitude differs between the two properties. However, the drive dependence can be quite different between the two experiments because of details of the geometry and shear properties of the soft layers that are excited differently.

Solid ^3He is soft but does not show NCRI: the two isotopes apparently possess similar elastic properties but different inertial properties. This isotopic dependence also would also appear to invalidate the present approach. However, thermal stress induced in the cooling/warming cycles is quite different because the thermal time constants differ considerably between the ^3He and ^4He solids. Also, the tunnelling motions of the dislocations are unlikely to be same.

Experiments can be performed to test the present model. Multiple-frequency TO resonators^{44,45} appear to give somewhat indecisive answers but still show the expected trend of enhanced NCRI at higher frequency. It is probable that damping should be included in the model to analyse these experiments in detail.

Shear modulus measurements have not been performed in a geometry for which the plastic flow lines would close on themselves in the way they do in torsional oscillators. Shear measurements between concentric cylinders could yield supersoft elastic moduli. The study of the resonance modes in simple acoustic cavities⁴⁶ constitutes a practical way to reveal the existence of an internal response in the sample.

The soft layers are relatively thick, possibly micron-thick.³⁶ The crystal lattice is heavily distorted and it is quite possible that the soft layers become genuinely superfluid. Superfluid behaviour mimicked here by infinite compliance is not described by the solutions of Eqs.(27a) and (22a) because the steady-state regime would never be reached. Dissipation must be taken into account. The influence of the viscoelastic behaviour discussed by Yoo and Dorsey²⁶ should be included in the model to extend its validity to large values of G/G_{eff} ,^{25,47} as can very well become necessary with the findings of future experiments.

- ¹ S. Trickey, W. Kirk, and E. Adams, Rev. Mod. Phys. **44**, 668 (1972).
- ² O. Penrose and L. Onsager, Phys. Rev. **104**, 576 (1956).
- ³ A. Andreev and I. Lifshits, Sov. Phys. JETP **29**, 1107 (1970).
- ⁴ G. Chester, Phys. Rev. A **2**, 256 (1970).
- ⁵ A. Leggett, Phys. Rev. Lett. **25**, 1543 (1970).
- ⁶ N. Prokof'ev, Advances in Physics, **56**, 381 (2007); S. Balibar and F. Caupin, J. Phys. Cond. Mat. **20**, 173201 (2008); D.E. Galli and L. Reatto, J. Phys. Soc. Jpn., **77**, 585 (2008).
- ⁷ L. Landau and E. Lifshitz, "Fluid mechanics," (Pergamon Press, London, 1959) Chap. XVI, p. 510.
- ⁸ E. Kim and M. Chan, Science **305**, 1941 (2004).
- ⁹ A. S. C. Rittner and J. D. Reppy, J. Low Temp. Phys. **101**, 155301 (2008).
- ¹⁰ J. T. West, O. Syshchenko, J. Beamish, and M. H. W. Chan, Nature Physics **5**, 598 (2009).
- ¹¹ S. Sasaki, F. Caupin, and S. Balibar, Phys. Rev. Lett. **99**, 205302 (2007).
- ¹² J. Day and J. Beamish, J. Low Temp. Phys. **148**, 627 (2007).
- ¹³ A. S. C. Rittner, W. Choi, E. J. Mueller, and J. D. Reppy, Phys. Rev. B **80**, 224516 (2009).
- ¹⁴ M. W. Ray and R. B. Hallock, Phys. Rev. B **79**, 224302 (2007).
- ¹⁵ S. Kwon, N. Mulders, and E. Kim, J. Low Temp. Phys. **158**, 590 (2010).
- ¹⁶ R. Wanner, I. Iwasa, and S. Wales, Solid State Com. **18**, 853 (1976).
- ¹⁷ V. L. Tsymbalenko, Soviet Physics JETP **47**, 787 (1978).
- ¹⁸ V. Tsymbalenko, Sov. Phys.-JLTP **49**, 859 (1979).
- ¹⁹ I. Iwasa, K. Araki, and H. Suzuki, J. Phys. Soc. Japan **46**, 1119 (1979).
- ²⁰ I. Iwasa and H. Suzuki, J. Phys. Soc. Jpn. **49**, 1722 (1980).
- ²¹ M.A. Paalanen, D.J. Bishop, and H.W. Dail, Phys. Rev. Lett. **46**, 664 (1981).
- ²² J. Day and J. Beamish, Nature (London) **450**, 853 (2007).
- ²³ J. Day and J. Beamish, J. Low Temp. Phys. **148**, 683 (2007).
- ²⁴ Y. Mukharsky, A. Penzev, and E. Varoquaux, Phys. Rev. B **80**, 140504 R (2009).
- ²⁵ X. Rojas, A. Haziot, V. Bapst, S. Balibar, and H. J. Maris, Phys. Rev. Lett. **105**, 145302 (2010).
- ²⁶ Z. Nussinov, A. V. Balatsky, M. J. Graf, and S. A. Trugman, Phys. Rev. B **76**, 014530 (2007); C.-D. Yoo and A. T. Dorsey, Phys. Rev. B **79**, 100504 (2009).
- ²⁷ I. Iwasa, Phys. Rev. B **81**, 104527 (2010).
- ²⁸ Y. Hiki and F. Tsuruoka, Phys. Lett. **62A**, 50 (1977).
- ²⁹ F. Tsuruoka and Y. Hiki, Phys. Rev. B **20**, 2702 (1979).
- ³⁰ A. Granato and K. Lüke, Appl. J. Phys. **27**, 583 (1956).
- ³¹ J. Day, O. Syshchenko, and J. Beamish, Phys. Rev. B **79**, 214524 (2009).
- ³² J. Day, O. Syshchenko, and J. Beamish, Phys. Rev. Lett. **104**, 075302 (2010).
- ³³ J. Friedel, *Dislocations*, first edition with corrections ed. (Pergamon Press, 1967) § 8.5.2.
- ³⁴ I. Iwasa, H. Suzuki, T. Suzuki, T. Nakajima, I. Yonenaga, H. Suzuki, H. Koizumi, Y. Nishio, and J. Ota, J. Low Temp. Phys. **100**, 147 (1995).
- ³⁵ J. Bossy, P. Bastie, P. Averbuch, O. Losserand, P. Courtois, I. Moukharshi, and A. Braslau, J. Low Temp. Phys. (2010).
- ³⁶ R. Amodeo and N. Ghoniem, Phys. Rev. B **41**, 6968 (1990).
- ³⁷ H. M. Zbib, M. Rhee, and J. P. Hirth, Int. J. Mech. Sci **40**, 113 (1998).
- ³⁸ O. Syshchenko, J. Day, and J. Beamish, Phys. Rev. Lett. **104**, 195301 (2010).
- ³⁹ Iwasa's simple relation²⁷ is not found here: the models are not equivalent. However, it seems to the present author that the relation between f_{NCRI} and G_{eff} reported by Iwasa²⁷ should stem from the results (9) and (13) for the homogeneous sample with G replaced by G_{eff} .
- ⁴⁰ A. S. C. Rittner and J. D. Reppy, J. Low Temp. Phys. **148**, 671 (2007).
- ⁴¹ A.C. Clark, J.D. Maynard, and M.H.W. Chan, Phys. Rev. B **77**, 184513 (2008).
- ⁴² A. Eyal and E. Polturak, J. Low Temp. Phys. , DOI 10.1007/s10909 (2011).
- ⁴³ D. Y. Kim, H. Choi, W. Choi, S. Kwon, E. Kim, and H. C. Kim, Phys. Rev. B **83**, 052503 (2011).
- ⁴⁴ Y. Aoki, X. Lin, and H. Kojima, J. Low Temp. Phys. **148**, 659 (2007).
- ⁴⁵ Y. Aoki, J. C. Graves, and H. Kojima, J. Low Temp. Phys. **150**, 252 (2008).
- ⁴⁶ Work in progress.
- ⁴⁷ H. J. Maris and S. Balibar, J. Low Temp. Phys. **160**, 5 (2010).